Front. Phys. 12(1), 127801 (2017)
DOI 10.1007/s11467-016-0612-3

RESEARCH ARTICLE

Silicon-erbium ytterbium silicate nanowire waveguides with optimized optical gain

Xiao-Xia Wang[1], Wei-Hao Zheng[1], Qing-Lin Zhang[1], Xiao-Li Zhu[1], Hong Zhou[1], Xiu-Juan Zhuang[1,*], An-Lian Pan[1,†], Xiang-Feng Duan[2]

[1] *Key Laboratory for Micro-Nano Physics and Technology of Hunan Province, School of Physics and Electronic Science, and State Key Laboratory of Chemo/Biosensing and Chemometrics, Hunan University, Changsha 410082, China*
[2] *Department of Chemistry and Biochemistry, University of California, Los Angeles, CA 90095, USA*
*Corresponding authors. E-mail: * zhuangxj@hnu.edu.cn, † anlian.pan@hnu.edu.cn*
Received July 12, 2016; accepted August 28, 2016

Single-crystal erbium silicate nanowires have attracted considerable attention because of their high optical gain. In this work, we report the controlled synthesis of silicon-erbium ytterbium silicate core-shell nanowires and fine-tuning the erbium mole fraction in the shell from $x = 0.3$ to $x = 1.0$, which corresponds to changing the erbium concentration from 4.8×10^{21} to 1.6×10^{22} cm^{-3}. By controlling and properly optimizing the composition of erbium and ytterbium in the nanowires, we can effectively suppress upconversion photoluminescence while simultaneously enhancing near-infrared emission. The composition-optimized nanowires have very long photoluminescence lifetimes and large emission cross-sections, which contribute to the high optical gain that we observed. We suspended these concentration-optimized nanowires in the air to measure and analyze their propagation loss and optical gain in the near-infrared communication band. Through systematic measurements using wires with different core sizes, we obtained a maximum net gain of 20 ± 8 dB·mm^{-1}, which occurs at a wavelength of 1534 nm, for a nanowire with a diameter of 600 nm and a silicon core diameter of 300 nm.

Keywords erbium ytterbium silicate, nanowire, erbium concentration, gain

PACS numbers 78.67.Uh, 42.70.-a, 81.07.Gf

1 Introduction

The optical properties of silicon-based, low-dimensional nanostructures in the near-infrared communication band are of considerable interest for the development of silicon-compatible integrated photonic circuits [1–7]. Unfortunately, the applicability of erbium-doped silicon or silica is largely limited by the low solid solubility of erbium (Er), which translates into doping concentrations of only 10^{16}–10^{20} cm^{-3} [8]. Recently, erbium silicates (Er_2SiO_5 and $Er_2Si_2O_7$) have attracted a great deal of attention, as they have a much higher erbium concentration (10^{22} cm^{-3}) than Er-doped Si-based materials [9, 10]. Single-crystalline erbium silicate nanowires (NWs) can serve as subwavelength optical waveguides with excellent gain performance, allowing optical amplification in the near-infrared communication band [11–14]. However, high optical gain is still difficult to achieve in pure erbium silicate NWs because of the concentration quenching effect and large upconversion (UC) emission, which can be directly inferred from the relatively short photoluminescence (PL) lifetime observed in these structures [15, 16]. Ytterbium (Yb) is introduced in erbium compounds to partly substitute the Er. It acts both as a disperser and a sensitizer, helping to suppress the PL quenching and the UC-induced low population inversion in the $^4I_{13/2}$ state of Er^{3+} [17, 18]. The relative concentration ratio of Er^{3+} to Yb^{3+} affects the gain properties of erbium-ytterbium silicate (EYS) nanowires. Wang *et al.* predicted that the net gain of single-crystal EYS NWs could reach values up to 27 dB·mm^{-1}, with a threshold as low as 0.7 mW [12].

The modal gain, G_{mod}, of a NW can be estimated by the following equation [19]:

$$\begin{aligned} G_{\mathrm{mod}} &= 4.34 \times \Gamma(\sigma_{\mathrm{em}} N_2 - \sigma_{\mathrm{abs}} N_1) \\ &\approx 4.34 \times \Gamma \sigma_{\mathrm{em}} N_{\mathrm{Er}}, \end{aligned} \tag{1}$$

where Γ is the optical confinement factor, σ_{em} and σ_{abs} are the emission and absorption cross-sections of the material, respectively, N_1 and N_2 are the Er concen-

© Higher Education Press and Springer-Verlag Berlin Heidelberg 2016

trations in the ground and excited state, respectively, and N_{Er} is the Er concentration in a gain medium. When assuming a 100% population inversion in the excited state, G_{mod} will be proportional to N_{Er}. Furthermore, the modal gain of a NW depends on not only the Er^{3+} concentration, but also the emission cross-section of Er^{3+} and the optical confinement of the light, especially for NWs with subwavelength diameters. In previous work, we designed and fabricated a silicon-erbium ytterbium silicate (Si-EYS) core–shell NW structure, with a high-refractive-index silicon core and a single-crystalline erbium–ytterbium silicate shell to achieve very good optical confinement of the guided light in the silicate shell [20]. We observed high optical amplification in the near-infrared communication band [20]. However, the optical losses induced by the substrate were neglected and the net gain value was overestimated in the previous measurements [20].

In this study, we synthesized a series of Si-EYS, Si-$(Er_xYb_{1-x})_2Si_2O_7$, core–shell NWs by tuning the Er concentration in the shell from 4.8×10^{21} to 1.6×10^{22} cm^{-3}. We found that when the mole fraction of Er, x, is optimized, we can effectively suppress UC emission while greatly enhancing near-infrared emission. For the erbium silicate nanowires, we have measured the longest lifetime of 2.8 ms to date, as well as very large emission cross-sections. Finally, we re-examined the propagation loss and net gain of the core–shell NWs with the wires suspended in the air. The results show that the suspended NWs can still exhibit prominent net gain at the wavelength of 1.53 μm. In particular, for a NW with a diameter of 600 nm and a silicon core diameter of 300 nm, we obtained a maximal net gain of ~20 dB·mm^{-1}.

2 Results and discussion

The as-grown NWs were several tens of micrometers in length and hundreds of nanometers in diameter, and had very smooth surfaces. A bright-field optical micrograph of a single Si-EYS NW with a length of ~30 μm and a diameter of ~600 nm is shown in Fig. 1(a), where both the smooth surface and the uniform diameter can be observed. Figure 1(b) shows the two-dimensional (2D) UC PL mapping of the single NW in the visible range, recorded under excitation by a continuous wave (CW) laser at 980 nm at room temperature. The fact that the emission intensities are uniform through the entire NW,

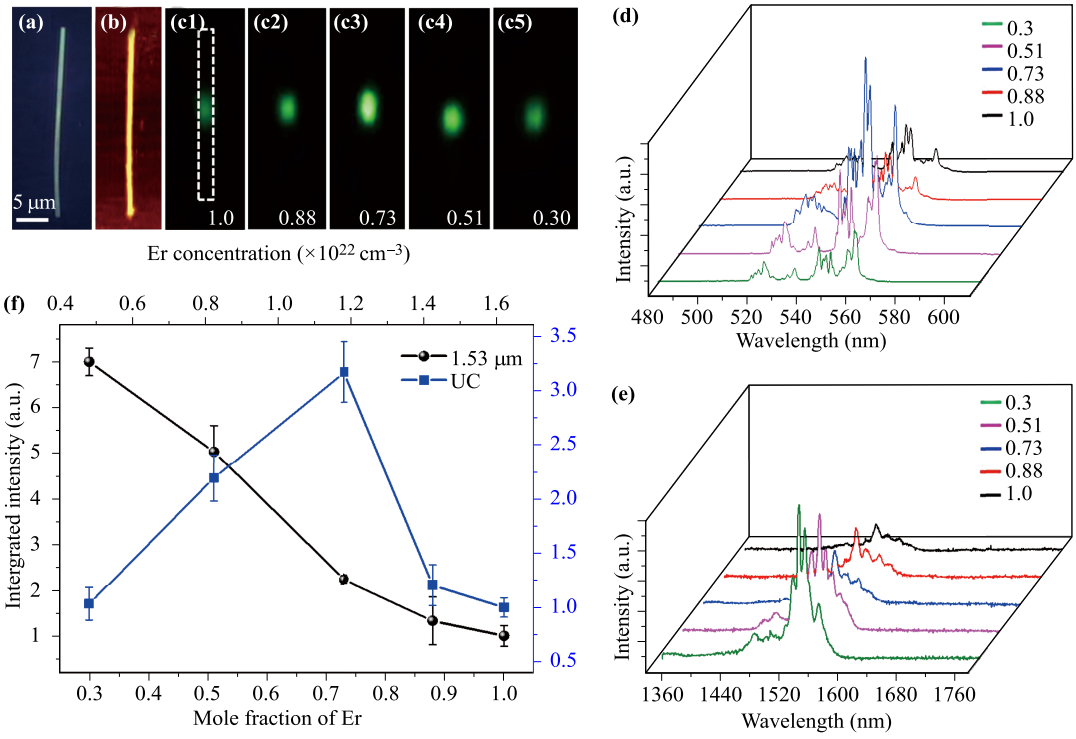

Fig. 1 **(a)** Bright-field optical micrograph of a single NW with Er mole fraction $x = 1.0$. **(b)** Two-dimensional mapping of the UC luminescence intensity for the wire in (a). **(c1–c5)** UC emission images of different NWs with mole fraction $x = 1$, 0.88, 0.73, 0.51, and 0.3. These pictures were taken under excitation by a 980 nm laser at room temperature. The laser spot diameter was ~5 μm. **(d)** UC emission spectra in visible range and **(e)** PL emission at 1.53 μm for the NWs shown in (c1–c5). **(f)** The UC (*blue squares*) and near-infrared emission intensity at 1.53 μm (*black circles*) as a function of the Er mole fraction.

indicates that the Er concentration is also uniform. Figures (c1–c5) are real-color photographs of single Si-EYS NWs with different mole fraction values ($x = 1.0 - 0.3$) under the same excitation intensity (~10 mW, CW laser at 980 nm). UC emission is mainly observed at 525 nm and 550 nm, wavelengths that correspond to the $^2H_{11/2}$–$^4I_{15/2}$ and $^4S_{3/2}$–$^4I_{15/2}$ transitions of Er^{3+}, respectively. Figures 1(d) and (e) show the UC and near-infrared PL spectra. The PL at 1.53 μm stems from the Er^{3+} radiative transitions from the first excited level $^4I_{13/2}$ to the ground state $^4I_{15/2}$. The $^4I_{13/2}$ energy level is usually more populated as a result of a nonradiative relaxation process from the $^4I_{11/2}$ state, which has a shorter lifetime. Figure 1(f) shows the PL intensities for both the UC and the 1.53 μm emission band of the Si-EYS NWs with the same size, as a function of the Er mole fraction. The intensity of the UC emission increases with the Er concentration, reaching its maximum value when $x = 0.73$, and then decreasing if the mole fraction of Er is further increased. However, the emission intensity at 1.53 μm reaches its maximum at a relatively low value of the Er mole fraction, $x = 0.3$. This maximum PL emission is about seven times stronger than the emission of the sample without Yb ($x = 1.0$). This result indicates that, for this optimized Er concentration (~4.8×10^{21} cm^{-3}), the UC effect can be effectively suppressed and the radiative emission at 1.53 μm can be greatly enhanced in the NWs.

According to the already established UC mechanism of the Er–Yb system, the energy transition process from Yb^{3+} to adjacent Er^{3+} plays a key role in UC luminescence [22, 23]. However, for the as-grown Si-EYS NWs with Er^{3+} concentrations up to ~10^{22} cm^{-3}, the Er^{3+}–Er^{3+} interaction becomes more efficient due to the greatly decreased Er^{3+}–Er^{3+} distance. Here, we need consider two different processes: the cooperative upconversion (CUC) and nonradiative cross-relaxation (CR) effects. CUC accounts for energy transfer between two nearby Er ions in excited states, whereas CR is related to the transfer from an excited Er^{3+} to an adjacent Er^{3+} in the ground state via a nonradiative mechanism. Consequently, CUC can increase the intensity of the UC emission, while CR tends to reduce it. The results in Fig. 1(f) demonstrate that CUC may be dominant when the Er^{3+} concentration is lower than 1.2×10^{22} cm^{-3} ($x = 0.73$), but gets suppressed for higher Er concentrations.

Figure 2 shows the PL lifetimes at 1.53 μm (under excitation by a 980 nm pulse laser) as a function of the Er mole fraction, and the inset depicts the decay curves of the samples for different values of x. The lifetime increased by approximately four fold, from 100 μs to 2.8 ms, when the Er concentration decreased from $x = 1.0$ to $x = 0.3$. Such a significant enhancement of the lifetime can be explained by the decrease in the number of nonradiative recombination channels, which may be related to a reduction of the Er^{3+} concentration quenching effect for high Yb^{3+} concentrations. Note that the lifetimes are much longer than the reported values of 5.7 and 20 μs for Er_2O_3 and Er_2SiO_5, respectively [23, 24]. The 2.8 ms lifetime exhibited by the NWs with an Er^{3+} concentration of 4.8×10^{21} cm^{-3} is longer than the reported value (1.8 ms) for erbium yttrium chloride silicate NWs [14]. This is the longest lifetime measured in erbium silicate nanowires so far. These long PL lifetimes can provide the base for the effective suppression of UC, and make population inversion much easier to realize under typical pumping power, which is critical to achieve a large net gain.

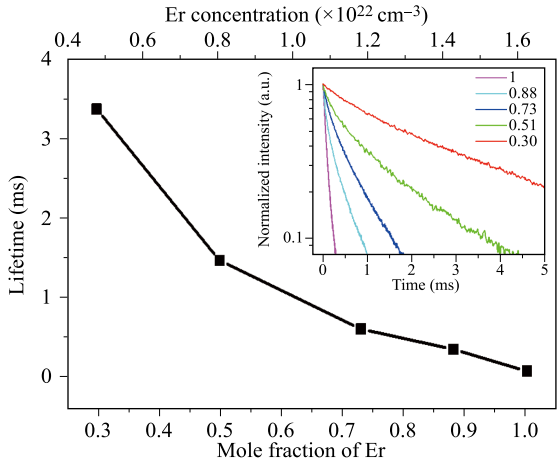

Fig. 2 Lifetimes as a function of the Er mole fraction for near-infrared emission at 1.53 μm, under excitation by a 980 nm pulse laser. The inset shows the decay curves at 1.53 μm for samples with different Er mole fraction.

We measured the propagation loss and net gain of Si-EYS core–shell NWs with the optimal Er^{3+} concentration (4.8×10^{21} cm^{-3}). As shown in our previous paper [20], the relative gain is given by the following equation:

$$G_r = 10\log(I_{\text{p-on}}/I_{\text{p-off}}) = a + G_{\text{mod}}, \tag{2}$$

where $I_{\text{p-on}}$ and $I_{\text{p-off}}$ are the intensities of the output signal with the pump laser on and off, respectively. The value of G_r includes the modal absorption a and the modal gain G_{mod}. However, it is not appropriate to calculate the net gain value just as the difference between the relative gain and the total loss, measured at 1534 nm, when the NWs are on a substrate, as the latter also induces optical loss. Thus, to prevent the effect of the substrate, we conducted the loss and gain measurements by suspending wires in the air. Figure 3(a) shows a schematic of the propagation loss measurement for a suspended NW coupled with two optical fiber tapers. One end of the NW was fixed to a SiO_2 substrate using

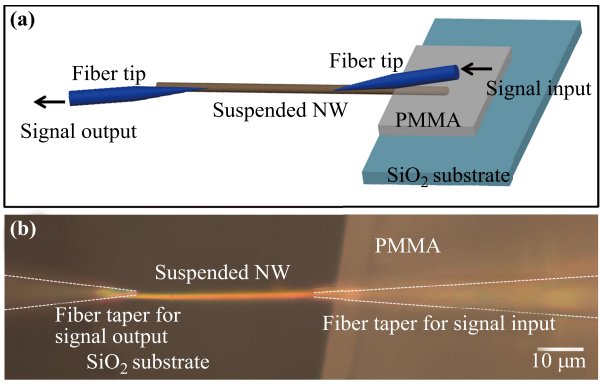

Fig. 3 **(a)** Schematic of the propagation loss measurement for a suspended NW. Two fiber tapers were used to input and output the light. The NW was suspended in the air by fixing one of its ends to PMMA on a SiO_2 substrate. **(b)** Photograph of a suspended Si-EYS NW. The length of the wire buried in PMMA and that suspended in the air were about 10–15 μm and 50 μm, respectively.

polymethyl methacrylate (PMMA), and the other end was suspended in the air. More details about the experimental setting can be found in the *Experiments* Section. Figure 3(b) shows the photograph of a suspended NW waveguide, and the lengths of wire that were buried in the PMMA and suspended in the air were about 15 and 50 μm, respectively.

The waveguide loss at 1590 nm was considered to be close to the propagation loss at 1534 nm, because at 1590 nm, there is almost no light absorption and the difference in wavelength between the two spectral positions is small enough. Figures 4(a) and (b) show the optical loss as a function of the transmitting length for NWs with a total diameter of 600 nm and core diameters of 0, 200, 300, and 400 nm, at 1534 nm and 1590 nm, respectively. Based on these results, we obtained both the total loss (α) and propagation loss (β) at 1534 nm and the values are listed in Table 1. We note that the total losses measured at 1534 nm were smaller than the previously measured values for NWs resting on a SiO_2 substrate [20] (because by suspending the NW waveguides in the air, we avoid the substrate-induced loss effects), but larger than the propagation loss detected at 1590 nm due to intrinsic material absorption at 1534 nm. The propagation losses at 1534 nm, for NWs with a total diameter of 600 nm and core diameters of 0, 200, 300, and 400 nm, were measured to be 72 ± 5, 34 ± 5, 26 ± 3, and 10 ± 2 dB·mm^{-1}, respectively. All these values are smaller than the results previously reported in Ref. [20].

The net gain can be obtained from the equation $G_n = G_r - \alpha_{1534}$, where α_{1534} is the total transmission loss at 1534 nm. The net gain values as a function of pumping power for three representative core sizes (200, 300, and 400 nm) are shown in Fig. 4(c), whereas Fig. 4(d)

Table 1 Total losses (α), propagation losses (β), and modal absorption ($a = \alpha - \beta$) at 1534 nm for Si-EYS core–shell NWs (in dB·mm^{-1}).

Core diameter (nm)	α	β	a
0	152 ± 8	72 ± 5	80 ± 13
200	109 ± 5	34 ± 5	75 ± 10
300	96 ± 5	26 ± 3	70 ± 8
400	72 ± 4	10 ± 2	62 ± 6

shows the dependence on the core size of the maximum net gain values (*black circles*) and the pumping threshold for positive net gain (*blue squares*). The optimal core size is approximately 300 nm. The NW with this core diameter value produces the best amplification performance, that is, the lowest net gain pumping threshold and the maximum net gain. The NW with a core diameter of 300 nm has a net gain of 20 ± 8 dB·mm^{-1}, which is slightly less than the previously reported value (31 dB·mm^{-1}) for the same wire geometry on the substrate [20], but still about fifteen times larger than that obtained for a microscale erbium–ytterbium codoped phosphate glass optical waveguide amplifier [25]. In particular, compared to the pure erbium chloride compound nanowire (with a relative gain of 64.4 dB·mm^{-1}, net gain of 3 dB·mm^{-1} in 900 nm diameter nanowires) [26], our core-shell nanowires exhibit considerably higher relative gain (115 dB·mm^{-1}) and net gain (20 dB·mm^{-1}) while at even smaller diameter of 600 nm (see Table 2). This highlights the importance of the core/shell structure design to enable the high optical gain, as reported in our original letter.

Using the above loss values and the relative gain previously reported [20], the modal absorption (a) can be obtained through the equation $a = \alpha_{1534} - \beta$. The modal absorptions for the above NWs with core diameters of 0, 200, 300, and 400 nm were calculated to be 80 ± 13, 75 ± 10, 70 ± 8, and 62 ± 6 dB·mm^{-1}, respectively (Table 1). Based on the above analysis, the absorption and emission cross sections of the material can be further es-

Table 2 Absorption (σ_{abs}) and emission (σ_{em}) cross-sections of an NW with a core diameter of 300 nm.

	This work	Er doped glass (Ref. [24])	Erbium chloride silicate NW (Ref. [26])
[a]N_{Er}	4.8×10^{21}	$10^{18} - 10^{19}$	1.62×10^{22}
[b]σ_{abs}	7.4×10^{-20}	6.0×10^{-21}	0.94×10^{-20}
[b]σ_{em}	8.1×10^{-20}	7.3×10^{-21}	–
[c]D	600	–	900
[d]G_r	115	–	64.4
[e]G_n	20		3

[a]Concentration of Er (unit: cm^{-3}), [b]Unit: cm^2, [c]Diameter of the nanowire(unit: nm), [d]Relative gain (unit: dB·mm^{-1}), [e]Net gain (unit: dB·mm^{-1}).

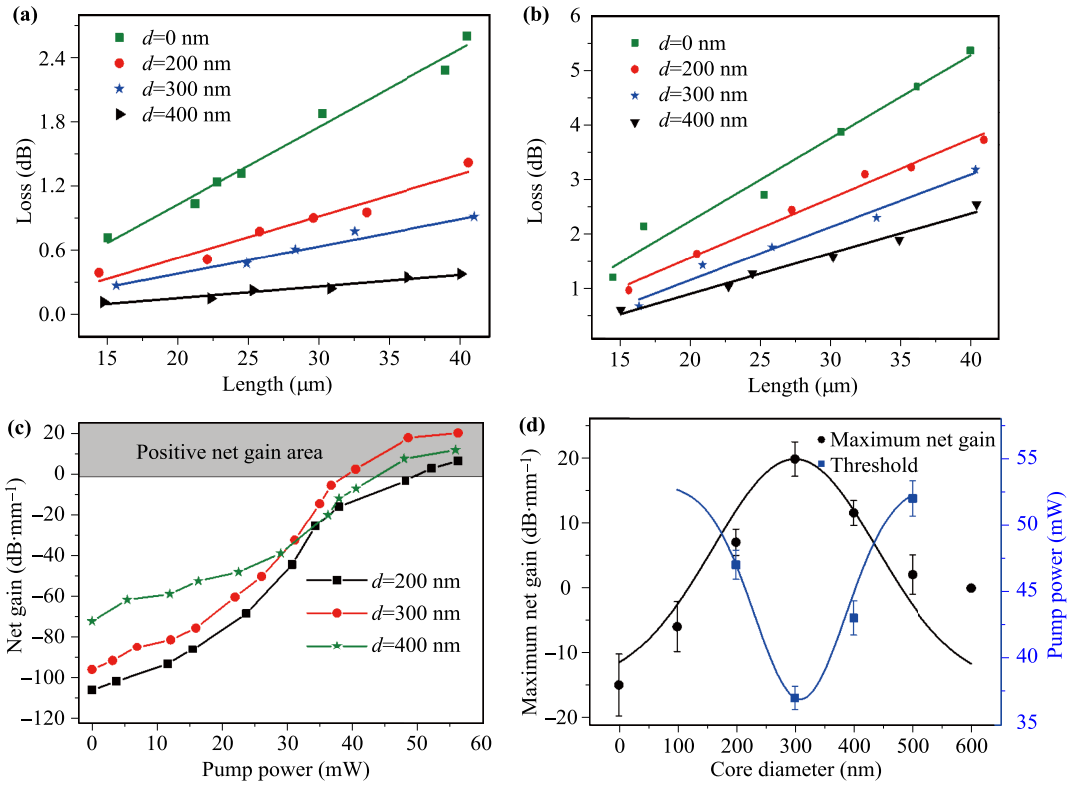

Fig. 4 **(a)** Loss as a function of the guided length at a wavelength of 1590 nm and along four different NWs, with a diameter of 600 nm and a core diameter of 0 nm (*green squares*), 200 nm (*red circles*), 300 nm (*blue stars*), and 400 nm (*black triangles*). Blue, red, and green lines represent the linear fit of the experimental data. **(b)** Loss as a function of the guided length at a wavelength of 1534 nm and along the four NWs in (b). **(c)** Net gain as a function of pump power for wires with core diameter $d = 200$, 300, and 400 nm. (The diameter of the wire is 600 nm.) **(d)** Maximum net gain (*black circles*, pumped at 56 mW) and positive net gain threshold (*blue squares*) for different diameters of the silicon core.

timated using the following expression [19]:

$$a = 4.34 \times \Gamma \sigma_{\mathrm{abs}} N_{\mathrm{Er}}, \tag{3}$$

where Γ and N_{Er} are 0.45 and 4.8×10^{21} cm^{-3}, respectively [20]. For example, we can use (3) to determine that the NW with core diameter of 300 nm has an absorption cross-section $\sigma_{\mathrm{abs}} = 7.4 \times 10^{-20}$ cm^2, which is about one order of magnitude larger than those for the Er^{3+} doped silicate glass material (6.0×10^{-21} cm^2 [24]; see also Table 2) as the absorption or emission cross-sections in a single crystal structure (such as $Er_xY_{2-x}SiO_5$) are usually larger than those in a polycrystalline structure, such as the Er^{3+} doped glass materials [16, 23, 24]. In addition, σ_{abs} is about seven times larger than the values for erbium chloride silicate NW with an Er concentration of 1.62×10^{22} cm^{-3} [26]. The emission cross-section of a material can be theoretically estimated using the McCumber theory once the absorption cross-section has been obtained [27]. By applying this, the emission cross-section σ_{em} for the NW with a core diameter of 300 nm was estimated to be 8.1×10^{-20} cm^2, which is about one order of magnitude larger than the values for the Er^{3+} doped silicate glass material (7.3×10^{-21} cm^2 [24]). Based on these absorption and emission cross-section values, the population inversion can be estimated to be about 60%, and this greatly contributes to the large net gain of the NWs.

3 Summary

We successfully synthesized Si-EYS core–shell NWs by tuning the Er concentration in the shell from 4.8×10^{21} to 1.6×10^{22} cm^{-3}. We measured the UC luminescence and near-infrared emission at 1.53 μm for different concentrations within this range, finding that when the concentration ratio of Er to Yb is set properly, the near-infrared emission can be up to seven times larger than that of a pure erbium silicate NW. A long PL lifetime of approximately 2.8 ms can be observed when the Er concentration is 4.8×10^{22} cm^{-3}. Using NWs with this optimal concentration, we systemically examined the loss and

net gain in the near-infrared communication band (1534 nm) with the wires suspended in the air. The results show that Si-EYS NWs can still achieve quite a large net gain, with a maximum value of around 20 ± 8 dB·mm^{-1}, achieved for a silicon core diameter of ∼300 nm. Si-EYS core–shell NWs exhibit a high-quality crystalline shell, large emission and absorption cross-sections, which further support the high net gain that we observed, and show great potential for application to Si-compatible integrated optoelectronics devices.

4 Experiments

Time-resolved PL measurements: Briefly, a mode-locked Ti:Sapphire laser (Tsunami) at 800 nm (pulse width 80 fs, repetition frequency 80 MHz) was amplified by a regenerative amplifier laser (Spitfire Ace 100, 1 kHz) and then was introduced into an optical parameter amplifier (OPA, TOPAS Prime). The laser output from the OPA can be continuously tuned from 300 to 2600 nm, and we used it at 980 nm (pulse width 80 fs, repetition frequency 1 kHz) to excite the sample. An infrared-extended photomultiplier tube (Hamamatsu, H10330B-75) is used to detect the time-resolved PL of the NWs.

Suspended NW fabrication: A PMMA solution was first dropped on the edge of a SiO_2 substrate using a capillary tube. Then, a NW was transferred there using a fiber taper controlled through a micro-manipulator. One end of the NW was embedded in the PMMA droplet and the remaining part was suspended in the air, as shown in Fig. 3(a). Finally, in order to dry the PMMA droplet, the substrate was placed in a drying closet at 60 °C for 10 min. It is worth noting that the PMMA acted as a kind of sticky solution to fix part of the NW on the SiO_2 substrate and that the length of the wire buried in PMMA was about 10–15 μm.

Loss measurements: The fabricated NW was placed under a microscope (Zeiss Axio Imager A2m) to perform the loss measurements. A tunable laser at 1520–1630 nm (Agilent-81949A) was coupled into a tapered single-mode fiber as the input signal [Input end in Fig. 3(a)]. The guided light from the other end of the wire was coupled into another tapered single-mode optical fiber and then captured by a spectrometer (Horiba 550) with an InGaAs detector cooled with liquid nitrogen. In our experiment, we used the evanescent field coupling method to shed light from the fiber taper into the NW and then couple light into the fiber taper at the other end of the wire. To calculate the loss at 1534 and 1590 nm, we performed a linear fit of a plot showing output signal intensity as a function of propagation length. The different propagation lengths were achieved by moving the launch-in fiber taper forward step by step along the length of the wire, and fixing the pick-up fiber taper at the other end of the wire. Both an infrared and a visible camera were used to monitor the light coupling process in order to maintain a constant coupling efficiency when the taper was moved forward.

Acknowledgements The authors are grateful to the National Natural Science Foundation of China (Grant Nos. 11374092, 61474040, 61574054, 61635001, and 61505051), the National Basic Research Program of China (Grant No. 2012CB933703), and the Aid Program for Science and Technology Innovative Research Team in Higher Educational Institutions of Hunan Province, the Hunan Provincial Science and Technology Department (Grant Nos. 2014FJ2001 and 2014GK3015).

References

1. F. Priolo, T. Gregorkiewicz, M. Galli, and T. F. Krauss, Silicon nanostructures for photonics and photovoltaics, *Nat. Nanotechnol.* 9(1), 19 (2014)
2. N. Liu, W. Y. Li, M. Pasta, and Y. Cui, Nanomaterials for electrochemical energy storage, *Front. Phys.* 9(3), 323 (2014)
3. R. L. Savio, M. Galli, M. Liscidini, L. C. Andreani, G. Franzò, F. Iacona, M. Miritello, A. Irrera, D. Sanfilippo, A. Piana, and F. Priolo, Photonic crystal light emitting diode based on Er and Si nanoclusters co-doped slot waveguide, *Appl. Phys. Lett.* 104, 121107 (2014)
4. R. M. Guo, X. J. Wang, K. Zang, B. Wang, L. Wang, L. Gao, and Z. Zhou, Optical amplification in Er/Yb silicate strip loaded waveguide, *Appl. Phys. Lett.* 99(16), 161115 (2011)
5. N. P. Dasgupta and P. D. Yang, Semiconductor nanowires for photovoltaic and photoelectrochemical energy conversion, *Front. Phys.* 9(3), 289 (2014)
6. H. S. Han, S. Y. Seo, J. H. Shin, and N. Park, Coefficient determination related to optical gain in erbium-doped silicon-rich silicon oxide waveguide amplifier, *Appl. Phys. Lett.* 81(20), 3720 (2002)
7. Lee, J. H. Shin, and N. Park, Optical gain at 1.5 μm in nanocrystal Si sensitized, Er-doped silica waveguide using top-pumping 470 nm LED, *J. Lightwave Technol.* 23, 19 (2005)
8. M. Miritello, R. Lo Savio, F. Iacona, G. Franzò, A. Irrera, A. M. Piro, C. Bongiorno, and F. Priolo, Efficient luminescence and energy transfer in erbium silicate thin films, *Adv. Mater.* 19(12), 1582 (2007)
9. H. Isshiki, M. J. A. de Dood, A. Polman, and T. Kimura, Self-assembled infrared-luminescent Er–Si–O crystallites on silicon, *Appl. Phys. Lett.* 85, 4343 (2004)
10. H. J. Choi, J. H. Shin, K. Suh, H. K. Seong, H. C. Han, and J. C. Lee, Self-organized growth of Si/Silica/$Er_2Si_2O_7$ core-shell nanowire heterostructures and their luminescence, *Nano Lett.* 5(12), 2432 (2005)

11. A. L. Pan, L. J. Yin, Z. C. Liu, M. H. Sun, R. B. Liu, P. L. Nichols, Y. G. Wang, and C. Z. Ning, Single-crystal erbium chloride silicate nanowires as a Si-compatible light emission material in communication wavelength, *Opt. Mater. Express* 1(7), 1202 (2011)
12. X. J. Wang, S. Wang, and Z. Zhou, Low threshold $Er_xYb(Y)_{2x}SiO_5$ nanowire waveguide amplifier, *Appl. Opt.* 54(9), 2501 (2015)
13. L. Yin, H. Ning, S. Turkdogan, Z. Liu, P. L. Nichols, and C. Z. Ning, Long lifetime, high density single-crystal erbium compound nanowires as a high optical gain material, *Appl. Phys. Lett.* 100(24), 241905 (2012)
14. L. Yin, D. Shelhammer, G. Zhao, Z. Liu, and C. Z. Ning, Erbium concentration control and optimization in erbium yttrium chloride silicate single crystal nanowires as a high gain material, *Appl. Phys. Lett.* 103(12), 121902 (2013)
15. C. P. Michael, H. B. Yuen, V. A. Sabnis, T. J. Johnson, R. Sewell, R. Smith, A. Jamora, A. Clark, S. Semans, P. B. Atanackovic, and O. Painter, Growth, processing, and optical properties of epitaxial Er_2O_3 on silicon, *Opt. Express* 16(24), 19649 (2008)
16. X. J. Wang, T. Nakajima, H. Isshiki, and T. Kimura, Fabrication and characterization of Er silicates on SiO_2/Si substrates, *Appl. Phys. Lett.* 95(4), 041906 (2009)
17. X. J. Wang, B. Wang, L. Wang, R. M. Guo, H. Isshiki, T. Kimura, and Z. Zhou, Extraordinary infrared photoluminescence efficiency of $Er_{0.1}Yb_{1.9}SiO_5$films on SiO_2/Si substrates, *Appl. Phys. Lett.* 98(7), 071903 (2011)
18. X. J. Wang, G. Yuan, H. Isshiki, T. Kimura, and Z. Zhou, Photoluminescence enhancement and high gain amplification of $Er_xY_{2x}SiO_5$ waveguide, *J. Appl. Phys.* 108(1), 013506 (2010)
19. S. A. Dimitri Geskus, S. Aravazhi, S. M. García-Blanco, and M. Pollnau, Giant optical gain in a rare-earth-ion-doped microstructure, *Adv. Mater.* 24, OP19 (2012)
20. X. X. Wang, X. J. Zhuang, S. Yang, Y. Chen, Q. L. Zhang, X. L. Zhu, H. Zhou, P. F. Guo, J. W. Liang, Y. Huang, A. L. Pan, and X. F. Duan, High gain submicrometer optical amplifier at near-infrared communication band, *Phys. Rev. Lett.* 115(2), 027403 (2015)
21. B. Wang, R. M. Guo, X. J. Wang, L. Wang, and Z. Zhou, Composition dependence of the Yb-participated strong up-conversions in polycrystalline ErYb silicate, *Opt. Mater.* 34(8), 1289 (2012)
22. P. Cardile, M. Miritello, and F. Priolo, Energy transfer mechanisms in Er-Yb-Y disilicate thin films, *Appl. Phys. Lett.* 100(25), 251913 (2012)
23. M. Miritello, P. Cardile, R. Lo Savio, and F. Priolo Energy transfer and enhanced 1540 nm emission in Erbium-Ytterbium disilicate thin films, *Opt. Express.* 19(21), 20761 (2011)
24. W. J. Miniscalco, Erbium-doped glasses for fiber amplifiers at 1500 nm, *J. Lightwave Technol.* 9(2), 234 (1991)
25. F. D. Patel, S. DiCarolis, P. Lum, S. Venkatesh, and J. N. Miller, A compact high-performance optical waveguide amplifier, *IEEE Photonics Technol. Lett.* 16(12), 2607 (2004)
26. Z. C. Liu, G. J. Zhao, L. J. Yin, and C. Z. Ning, Demonstration of Net Gain in an Erbium Chloride Silicate Single Nanowire Waveguide, Proceeding of Conference on Lasers and Electro-Optics: Science and Innovations, June 2014, San Jose, SM4H.4 (2014)
27. W. J. Miniscalco and R. S. Quimby, General procedure for the analysis of Er^{3+} cross sections, *Opt. Lett.* 16(4), 258 (1991)